

Time-resolved laser-induced desorption spectroscopy (LIDS) for quantified *in-situ* hydrogen isotope retention measurement and removal from plasma facing materials



Cite as: Rev. Sci. Instrum. 90, 073502 (2019); doi: 10.1063/1.5100162

Submitted: 15 April 2019 • Accepted: 18 June 2019 •

Published Online: 15 July 2019



View Online



Export Citation



CrossMark

J. H. Yu,^{a)} M. J. Baldwin, M. J. Simmonds, and A. Založnik

AFFILIATIONS

Center for Energy Research, University of California San Diego, La Jolla, California 92093-0417, USA

^{a)}Electronic mail: j2yu@eng.ucsd.edu

ABSTRACT

A laboratory scale laser induced thermal desorption spectroscopy system is developed and tested on tungsten-deuterium and titanium-deuterium codeposits, and its feasibility as a hydrogenic inventory measurement diagnostic is demonstrated over a range of retention values from $5 \times 10^{19} \text{ m}^{-2}$ to $7 \times 10^{23} \text{ m}^{-2}$ for absorbed laser power densities as low as 8 MW m^{-2} . Codeposit layer samples are grown by magnetron sputtering and immersed in a weak argon rf plasma. A 1 kW fiber laser ($\lambda = 1100 \text{ nm}$) heats the samples up to a peak surface temperature ranging from 900 to 1500 K using pulse widths of 0.5 and 1 s. Spectral line emission from Balmer series D α and H α from thermally desorbed deuterium and hydrogen, as well as line emission from argon, are monitored as a function of time using an optical spectrometer with maximum temporal resolution of 1 ms. To correct for wall recycling and pumping speed, and to accurately measure the time evolution of the laser-induced thermal desorption, the raw D α signal is deconvolved with the system response function, which is obtained by injecting a short burst of D $_2$ to approximate an impulse. Calibration is done with a standard D $_2$ leak, and laser induced desorption spectroscopy deuterium retention values are found to be in good agreement with companion measurements made using conventional temperature programmed desorption on samples from the same codeposit batch.

Published under license by AIP Publishing. <https://doi.org/10.1063/1.5100162>

I. INTRODUCTION

In nuclear fusion devices, the interaction of the edge plasma with plasma facing components (PFCs) leads to various effects. Such effects include surface erosion by sputtering, layer growth from the redeposition of sputtered PFC material, and trapping of deuterium (D) and tritium (T) fuel species within the PFC material or the deposited layers (commonly referred to as codeposits). For the nuclear fusion endeavor, fuel trapping, or rather the loss of T from the fuel cycle, is problematic as T management practice must satisfy low in-vessel limits to meet the requirements of both nuclear safety licensing and tritium breeding.¹ As a consequence, strategies are required for T inventory assessment and control in fusion reactor PFCs, and diagnostic capabilities that can measure and/or remove T from plasma-wetted surfaces and material deposition

areas are currently high priority research tasks in ongoing fusion research.²

There are few reliable methods for quantifying hydrogen (H) isotopes in material surfaces. Nuclear reaction analysis (NRA)^{3,4} is a widely used technique for such measurements, utilizing high energy projectile ions to form detectable nuclear products from subsurface target species such as H, but NRA is not suitable as an in-vessel fusion diagnostic due to the need for a typically large accelerator to produce the high energy ion beam. Recently, there has been a renewed interest in laser-based methods combined with optical spectroscopy⁵⁻⁷ to locally measure and remove hydrogenic species from materials *in situ*, including laser induced breakdown spectroscopy (LIBS),⁸⁻¹⁵ laser induced ablation spectroscopy (LIAS),^{16,17} and laser induced desorption spectroscopy (LIDS).¹⁸⁻²⁰ With LIBS, high peak power densities achievable with short pulse lasers

(femtoseconds to tens of nanoseconds) create a laser-induced plasma from ablated materials, which is characterized spectroscopically. In contrast, LIAS and LIDS employ an external plasma to excite laser-desorbed material for spectroscopic identification and quantification. Lasers with intensity below the ablation threshold, such as those used in LIDS, release trapped hydrogenic species from materials via thermal desorption without destruction of the material surface.

In fusion applications, laser-induced release of gas from stainless steel was first investigated by Schwirzke²¹ using measurements of pressure rise to infer released gas quantities, but no identification of the released gas was made. Further development^{22,23} of laser desorption has progressed using various detection schemes to measure desorbed species, including a time-of-flight mass spectrometer,²⁴ a quadrupole mass spectrometer (QMS),²⁵ a QMS in conjunction with NRA,²⁶ and temperature programmed desorption (TPD) before and after laser heating.²⁷ Pioneering LIDS work at the TEXTOR tokamak used the edge plasma to excite laser-desorbed deuterium and a CCD camera and an interference filter to detect Da optical emission.^{6,18–20} In that work, the laser pulse width was 1–10 ms, which provided spatial control of heat deposition by limiting lateral heat diffusion.

In this article, we explore LIDS as a diagnostic system with the potential for targeted, *in situ*, hydrogen isotope measurement in and removal from PFC surfaces and present a new analysis method for LIDS data. The experimental setup for time-resolved LIDS is outlined and we describe a deconvolution analysis technique which corrects for the repeated interchange of hydrogenic species between the vessel wall and the plasma, a process known as wall recycling.²⁸ Deconvolution provides an accurate measurement of the time-evolution of desorption, which is necessary if comparing LIDS data with hydrogen diffusion reaction models. The use of deconvolution is not limited to LIDS but can also be applied to any detection scheme where recycling, or other time-dependent system effects, alters the detected signal.

The LIDS system described here differs from other LIDS measurements^{6,18–20} in one or more of the following ways: (1) the spectral resolution of the spectrometer allows separation of Da and Ha using spectral fitting, (2) the temporal resolution of the spectrometer is sufficiently high relative to the laser pulse width to allow for a time-resolved measurement of desorption, (3) a calibrated D₂ leak located near the laser-irradiated area provides quantitative measurements of desorbed deuterium, eliminating the need for precise knowledge of spatially dependent plasma parameters required for the S/XB technique and eliminating the need for the optical field of view to cover the entire region of Da emission, (4) the system response function is measured experimentally using an impulsive burst of D₂ gas injection, and (5) numerical deconvolution of the measured signal with the system response function provides a correction for system-dependent time effects such as wall recycling and the finite pumping speed.

II. CODEPOSIT PREPARATION

Both titanium–deuterium (Ti–D) and tungsten–deuterium (W–D) codeposit layers were created for LIDS experiments in the present work. The Ti–D codeposits were used to provide good signals during LIDS by taking advantage of the high storage capacity of titanium thin films, leading to a large hydrogenic release

for optical detection and measurement. The second case of W–D codeposits demonstrated the technique on a fusion relevant material and showed that the technique can be used on materials with significantly less D inventory than that in Ti.

Identical Ti–D codeposit samples were prepared by magnetron sputtering of Ti targets with an argon sputtering plasma, using Ar fill pressure of 5 mTorr while simultaneously injecting D₂ with a fill pressure of 2.5 mTorr. Two batches of Ti–D codeposits were created using 25 mm diameter and 2 mm thick nickel discs as substrates, with codeposit layer thicknesses of 1.0 and 4.0 μm , both with surface temperature <500 K during deposition. Batches of identical W–D codeposits were also prepared by magnetron sputtering in an argon–deuterium mixture with 0.5 mTorr of Ar fill pressure and 9.5 mTorr of D₂, and surface temperature <350 K. The substrates for W–D layers were chosen to be 6 mm diameter W discs with thickness of 1.5 mm. The reason for using smaller substrates was to laser-heat the entire sample surface during LIDS, removing uncertainty about the area of desorption. Three batches of W–D codeposits were created with layer thickness ranging from 1.2 to 4.6 μm . Layer thicknesses were determined from mass gain by weighing samples before and after deposition.

One sample from each batch was analyzed for D content using TPD, in which samples were separately heated in the TPD oven at a rate of 0.3 K/s or 0.5 K/s from 300 to 1200 K, while monitoring the released D₂, HD, and H₂ with a residual gas analyzer which was calibrated with a known D₂ leak rate. A background subtraction method²⁷ was used to eliminate contribution to the HD and D₂ signals arising from water vapor in the TPD system, and the sensitivity for HD was assumed to be the same as that for D₂.

III. LASER, PLASMA, AND SPECTROMETER

The codeposited samples were immersed one at a time in an inductively coupled rf (13.56 MHz) plasma in argon, with steady-state rf power of 1000, 1500, and 2000 W used for each different sample. The plasma density and electron temperature were measured with a Langmuir probe and were $5\text{--}9 \times 10^{16} \text{ m}^{-3}$ and 3–4 eV, respectively. A fiber laser (Coherent Highlight 1000FL) with a wavelength of 1100 nm, a rectangular temporal shape, and an approximately Gaussian spatial profile was used to heat the samples during LIDS. Samples were air-cooled from the backside and the sample temperature was below 320 K immediately before laser irradiation. The gate valve to the vacuum turbo pump was kept open throughout the LIDS measurement. Electrons in the background argon plasma ionized, dissociated, and excited laser-desorbed deuterium gas for spectroscopic measurement. A 2-color pyrometer monitored the sample surface temperature during laser induced desorption, and a spectrometer (Avantes AvaSpec ULS2048) was used to measure Balmer series Da and Ha emission, as well as Ar I line emission. Figure 1 shows the experimental setup of the fiber laser, plasma chamber, spectrometer, pyrometer, and calibrated D₂ source (Laco Technologies) providing a flow rate of $5.2 \times 10^{16} \text{ D/s}$. RF power was coupled to the plasma from helicon antennae encircling a quartz bell jar, located approximately 30 cm above the sample. Plasma density decreased as a function of the axial distance (z) from the antennae due to the fact that the ionization source was localized near the antennae. This decrease in plasma density is shown in Fig. 2, which shows measurements of electron density, n_e , and

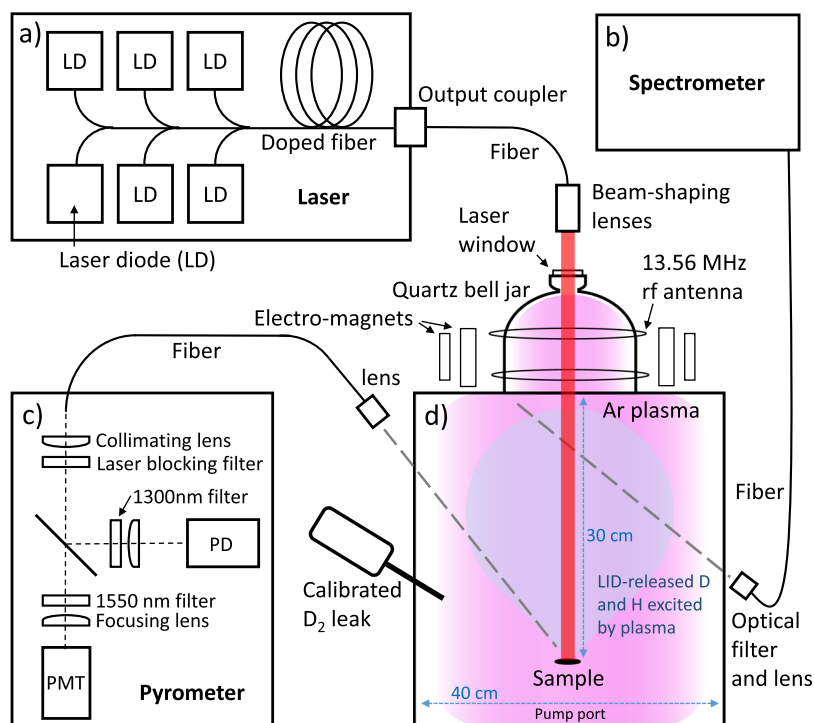


FIG. 1. Schematic of experimental setup for LIDS: (a) fiber laser, (b) spectrometer, (c) pyrometer, and (d) rf plasma chamber with calibrated D_2 leak.

electron temperature, T_e , both measured with a Langmuir probe, as well as measurements of Ar I and Ar II spectral line intensity, converted to spectral radiance using a calibrated light source (Optronic Laboratories 455-12 integrating sphere). The argon line

emission has a similar z -dependence as electron density, which is expected for relatively homogeneous T_e as in the rf plasma. Due to the higher electron density near the bell jar and thus larger spectroscopic signal-to-noise, the spectrometer was aimed in the upward direction at an angle of 30° with respect to horizontal during LIDS measurements.

In the case of Ti-D codeposits, the laser spot diameter on the samples was varied from 2.5 to 3.5 mm as measured by laser burn paper, and the absorbed laser power densities ranged from 20 to 100 $MW\ m^{-2}$. For these samples, the laser spot size was smaller than the sample size of 25 mm diameter. Lateral heat diffusion during the laser pulse was a source of uncertainty on the exact desorbed surface area, which depended on both the laser intensity and the pulse width. To avoid this uncertainty, smaller sample sizes of 6 mm diameter were used in the case of W-D codeposits, and the laser spot size was increased to 10 mm in order to cover the entire sample and to provide a relatively uniform irradiation across the sample. From the center of the sample to the edge, the laser intensity variation was approximately 25% as measured with a camera imaging diffusely reflected laser light. Temperature-independent reflectivities of 0.56²⁹ and 0.63^{29,30} were assumed for Ti and W, respectively, when quoting absorbed power densities in the present paper.

A fast pyrometer built in-house³¹ was used to detect thermal emission from the sample surface to measure surface temperature evolution during LIDS. An optical filter that transmitted $\lambda > 1200$ nm was used to block unwanted laser light. The light was then split using a beam splitter and passed through interference filters, each with a spectral bandwidth of 100 nm, and a photodiode (PD) and a photomultiplier tube (PMT) were used to detect 1300 and 1550 nm radiation, respectively. Additional neutral density

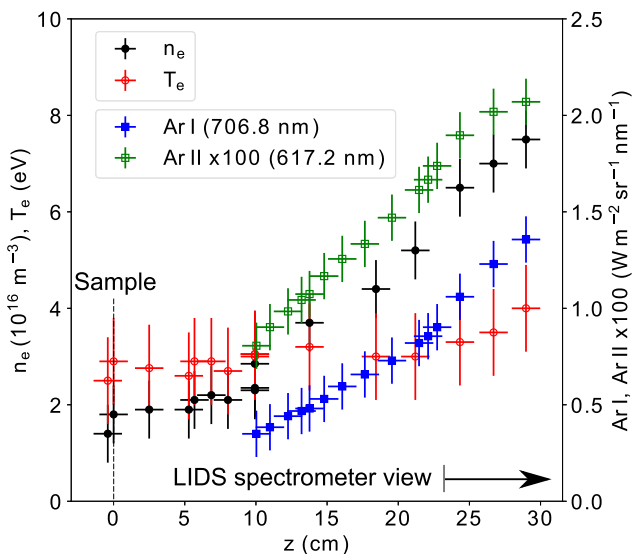


FIG. 2. Plasma parameters, n_e and T_e , and the spectral radiance from line-integrated measurements of Ar I and Ar II spectral lines, measured as a function of height in the rf plasma chamber with rf power of 1500 W and Ar fill pressure of 10.6 mTorr.

filters were used in front of the PMT as needed to avoid saturation. The temporal resolution of the PD depended on the gain and was typically <1 ms, while the PMT had a faster response of ~ 10 μ s. The pyrometer was calibrated using a W strip lamp with a known temperature as a function of lamp current. A 2-color method was used to calculate the surface temperature (avoiding the need to know absolute emissivity), which relies on the assumptions that the ratio of the sample emissivities at the two measured wavelengths during the actual measurement was the same as that during the calibration and that the ratio of emissivities does not change as a function of surface temperature.

IV. SPECTROSCOPY OF DESORBED DEUTERIUM

A. Spectral fitting

The Avantes spectrometer resolution of 0.35 nm near the wavelength of hydrogenic alpha emission was not sufficient to distinguish the peaks from Da (656.10 nm) and Ha (656.28 nm). This meant that sources of H (water vapor is always a contributor) would alter the measured amplitude and shape of the Balmer line observed during the LIDS pulse. The issue was addressed by separating the D and H contributions using a spectral fitting procedure that used experimentally determined spectra for Da and Ha separately. We fit the measured spectrum near 656 nm with a linear superposition of two functions,

$$S(\lambda) = a_D f_D(\lambda) + a_H f_H(\lambda),$$

where S is the modeled spectrum, a_D and a_H are fitting parameters for the amplitudes of Da and Ha, respectively, and the functions f_D and f_H are the measured spectra when pure D₂ or pure H₂ is injected into the Ar plasma, respectively, normalized to unity amplitude. These functions are the spectrometer response to each species and are fixed during the fitting procedure, that is, the only fitting parameters are a_D and a_H . Note that this method does not rely on choosing an appropriate analytic function for the line shapes because the functions are obtained from actual measurements. In the case of D₂ injection, the Da signal is orders of magnitude larger than the inherent background Ha signal. Examples of this technique are shown in Fig. 3 for two ratios of D/H, displaying an excellent agreement between the model and the data. The fit is performed for each spectral scan, which yields the time evolution of a_D and a_H separately.

B. Deconvolution and calibration

Here, we present a LIDS analysis technique which does not require precise knowledge of plasma parameters or detailed knowledge of particle-wall interactions such as the wall recycling coefficient. Ideally, when D₂ is desorbed from the target surface during the LIDS flash, the Da spectroscopic signal depends on the dissociation efficiency of D₂ and the excitation cross section for D in the background Ar plasma. Then, use of a calibrated D₂ flow into the same Ar plasma used during the LID event would allow for straightforward conversion of the optical data into D₂ molecular flow from the target surface, as plasma effects and the light collection efficiency are the same in each case. However, one challenge to accurately measuring time-resolved LIDS signals is that a desorbed particle can

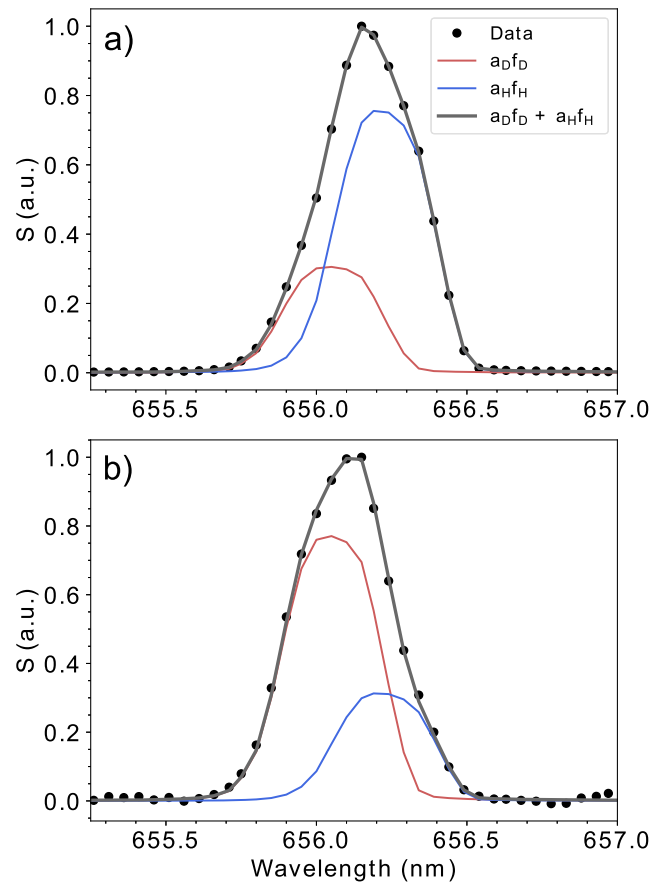


FIG. 3. (a) Spectral fitting for $a_D/a_H = 0.4$, (b): $a_D/a_H = 2.5$.

be counted multiple times due to wall recycling. In addition, the pumping speed of the vacuum system influences the magnitude and temporal shape of the detected D signal. A deconvolution approach to the data analysis was therefore necessary to address these issues.

Figure 4 shows the effect of wall recycling and limited pumping speed during calibration with a D₂ leak source. These system effects are evident as an increasing Da signal (red data points) with time after a constant D₂ flow from the calibrated leak was switched on ($t = 25$ s). To correct for these effects, we use the fact that the measured Da amplitude $a_D(t)$ is a convolution of the true D₂ flow rate f , and a system-dependent response function, g , given by

$$a_D(t) = c \int_{-\infty}^{\infty} f(\tau) g(t - \tau) d\tau,$$

where c is related to the manufacturer calibration of the constant leak source of D₂. The response function g contains all time-dependent effects of the entire system including wall recycling and pumping speed.

The system response is measured by injecting a quick burst of D₂ gas into the chamber (orange data points in Fig. 4) with identical background plasma conditions used during the calibration and LIDS events. The burst approximates an impulse function $\delta(t)$, which

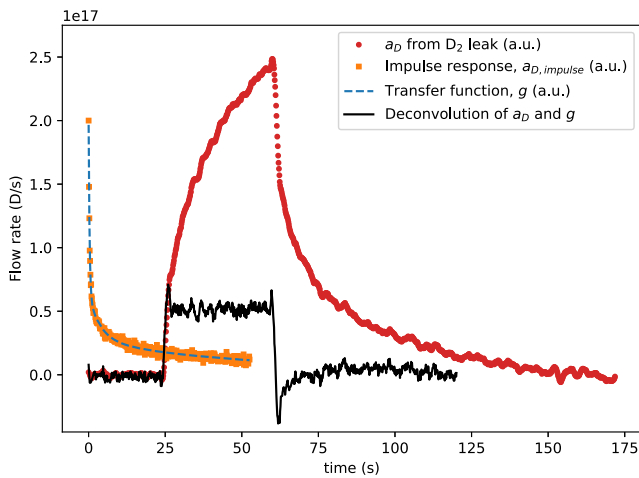


FIG. 4. Calibrated, steady, D_2 flow from $t = 25$ s through $t = 62$ s. Red data points are the measured $D\alpha$ amplitude, which increases due to wall recycling. Transfer function (blue dashed line) obtained from fit to $D\alpha$ immediately following short pulse of D_2 gas injection (orange squares), done after steady D_2 leak. Deconvolution (black) recovers actual flow rate.

allows the response function g to be directly measured using the following expression:

$$\int_{-\infty}^{\infty} \delta(\tau)g(t - \tau)d\tau = g(t),$$

that is, the measured signal from an impulse function is the system response function itself. We inject a sufficient amount of D_2 to give good signal to noise, but not enough to cause perturbation to the background plasma, which we verify by monitoring an Ar I emission line. To reduce noise in the deconvolution, the system response is fit with the sum of three exponential decay functions (blue curve).

Once the response function is known, it is then used to obtain the true flow rate (black curve) by deconvolving the measured signal (red) with the response (blue). It is noted that that the numerically deconvolved signal during the calibration flow is reasonably constant as is expected for the D_2 leak. The calibration factor, c , is the proportionality constant between the known calibrated flow rate and the normalized deconvolution. It is clear that failing to take time-dependent system effects into account can lead to misleading measurements (compare red and black curves). However, deconvolution typically degrades the signal-to-noise ratio of the original signal and can also lead to artifacts such as the overshoot seen in Fig. 4 when the flow is stopped ($t = 62$ s). We have used inverse filtering (shown here) and Fourier deconvolution algorithms, both with similar results.

The same deconvolution procedure is applied to data obtained during LIDS flash events to obtain the true temporal form of the LID release from targets. To analyze the LIDS $D\alpha$ signal, flow calibration and D_2 burst injection (to measure g) should be done shortly after the LIDS measurement while the wall conditions are similar as that during LIDS. We deconvolve the raw $D\alpha$ LIDS signal with g and use the same calibration factor obtained from the calibrated flow to convert the deconvolution into an actual flow rate of laser-desorbed deuterium. To determine desorbed flux, the flow rate is divided by

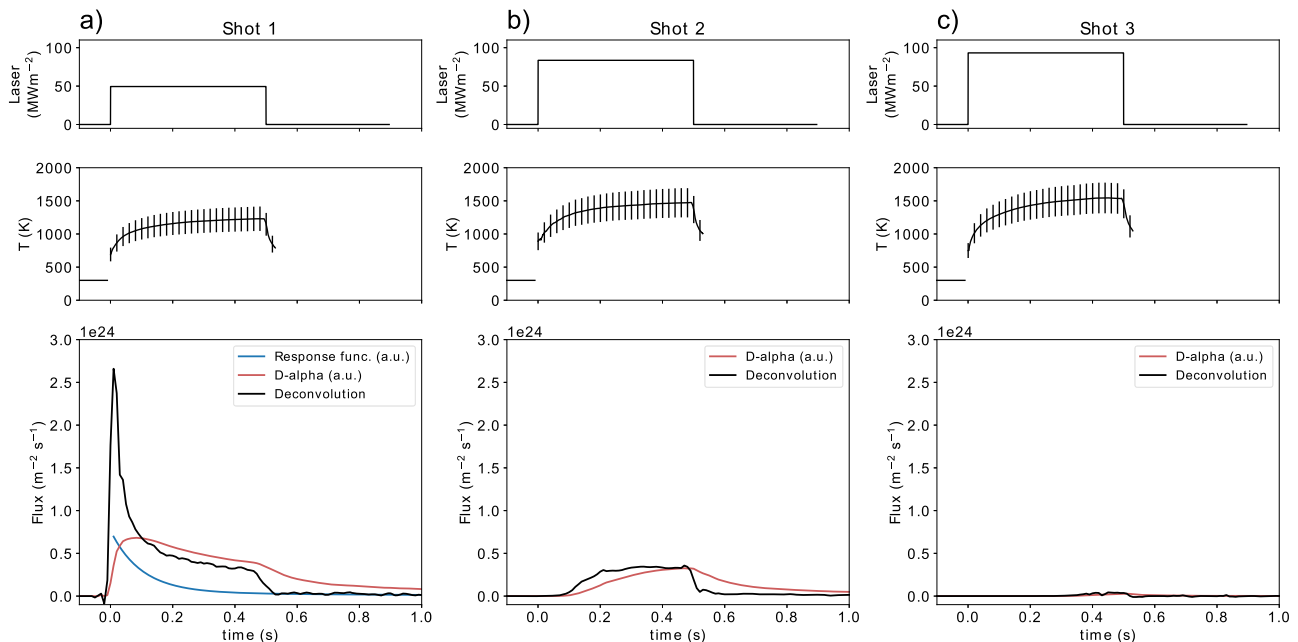


FIG. 5. LIDS data for three sequential 0.5 s laser irradiations of a $4 \mu\text{m}$ Ti-D codeposit layer in the same location, with increasing laser power density from shot-to-shot. Data shown: laser power pulse waveform (top), pyrometer surface temperature measurement (middle), and $D\alpha$ emission (bottom) during LIDS (red), system response function measured offline after LIDS (blue), and the calibrated deconvolution (black) of the response function and $D\alpha$. The inferred areal D released corresponds to an areal D retention of $4.4 \pm 0.9 \times 10^{23} \text{ m}^{-2}$, and TPD measurement on a sample from the same codeposit batch is $3.8 \pm 0.6 \times 10^{23} \text{ m}^{-2}$.

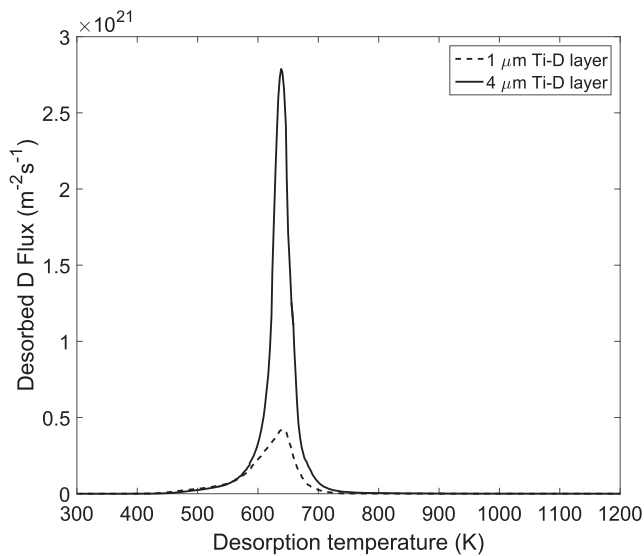


FIG. 6. TPD using a temperature ramp rate of 0.3 K s^{-1} for two Ti-D codeposits, both created with sample temperature of $\sim 500 \text{ K}$.

the laser-irradiated area, and retention is found by time-integrating the flux until the end of the heat duration.

V. CHARACTERIZATION OF TIME-RESOLVED LIDS

A. Ti-D codeposits

LIDS datasets for the Ti-D codeposit layer are shown in Fig. 5 for an irradiated laser spot of diameter 3.5 mm and pulse width of 0.5 s. The columns in Fig. 5 depict three separate laser irradiations of the same sample location. The top row shows the laser waveform, the middle row shows the pyrometer surface temperature measurement, and the bottom row shows the response function of the system (measured after LIDS), the raw D α emission, and the calibrated deconvolution. In this sequence of laser shots, the laser power was successively increased to obtain full removal of D as demonstrated by the lack of D emission following the second LIDS pulse. The difference in the temporal shape of the raw D α signal (red) compared to the corrected signal obtained by deconvolution (black) is striking, particularly when a large quantity of D is desorbed as in Fig. 5(a). The raw D α signal remains elevated after the laser pulse is finished even though the desorbed flux from the sample is zero. This is due to wall recycling, which effectively increases the pump out time for

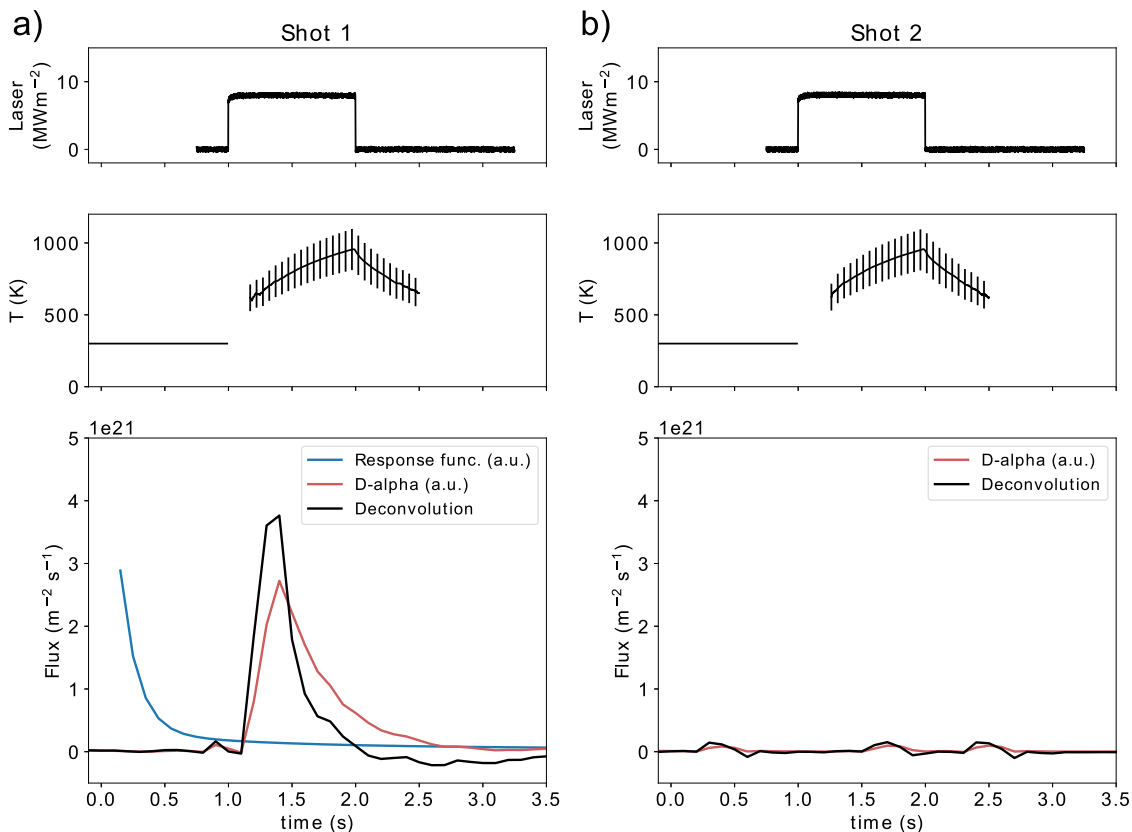


FIG. 7. Two successive LIDS measurements with 1 s pulses on $1.2 \mu\text{m}$ thick W-D codeposit with sample diameter 6 mm and laser spot diameter 10 mm. Data shown: laser power pulse waveform (top), pyrometer surface temperature measurement (middle), and D α emission (bottom) during LIDS (red), system response function measured offline after LIDS (blue), and the calibrated deconvolution of the response function and D α (black). The inferred areal D retention is $1.3 \pm 0.4 \times 10^{21} \text{ m}^{-2}$, in excellent agreement with conventional TPD analysis, as shown in Fig. 8.

deuterium released during the laser pulse. In contrast, the deconvolved signal, which is a true signal of desorbed D flux, falls to zero when the sample cools.

When calibrated, the released areal D gives a D retention value of $4.4 \pm 0.9 \times 10^{23} \text{ m}^{-2}$. The LIDS measure of D retention is found to agree within experimental error with that obtained on the control sample from the same codeposit batch, measured by conventional TPD. The largest source of uncertainty in determining the flux of D (and thus retention) for the Ti–D codeposits was the area of desorption, which was determined by measuring the diameter of laser-heat-induced discoloration using a laser confocal microscope.

Figure 6 shows the TPD measurements from a 1 and a 4 μm thick layer; the latter was created in the same codeposit batch as the LIDS sample in Fig. 5. TPD reveals a sharp release peak for the 4 μm layer at $\sim 630 \text{ K}$ and total areal D retention of $3.8 \pm 0.6 \times 10^{23} \text{ m}^{-2}$ which corresponds to a D/Ti ratio of approximately 0.6, indicating the layer is predominantly TiD_2 . The 1 μm sample had a lower D inventory with the TPD integral yielding a D retention of $1.1 \pm 0.3 \times 10^{23} \text{ m}^{-2}$. LIDS was performed on 25 mm diameter samples from this 1 μm layer coating as well, yielding retention values in agreement within error bars with the TPD value. The long tail in temporal shape of the deconvolved LIDS signal in Fig. 5 compared to the narrow release peak in the TPD measurement was due to the fact that the temperature was roughly constant in the LIDS data, which gives continual release of D from hydride decomposition.³²

B. W–D codeposits

Tungsten will be used as a plasma facing material in future tokamaks such as ITER and DEMO, and here, we show LIDS measurements of D retention in W–D codeposits. The trapping and thus desorption physics are different for W–D compared to Ti–D layers; hydrides are formed in Ti–D, while in W–D, deuterium is trapped at defects such as dislocations, monovacancies, and vacancy clusters, each with its own detrapping energy.³³ The sharp release peak of D from Ti–D occurs because when the temperature is sufficient to break hydride bonds, D rapidly diffuses to the surface and escapes. In contrast, the broader release peak from W–D is due to a multiple step process of thermally activated detrapping, diffusion of deuterium through the material, and repeated trapping and detrapping. A time-resolved measurement of desorbed D, as is presented here, is critical for accurate modeling of this multistep desorption process.

The quantified LIDS measurement and removal of D from W–D codeposits is demonstrated by comparison of the data presented in Figs. 7 and 8. These data represent D release from separate targets from a batch of identical 1.2 μm thick magnetron sputtered W–D codeposit layers prepared on W substrates at 330 K. Figure 7 shows laser-induced thermal release measured by LIDS, while Fig. 8 gives companion data from conventional TPD. The TPD desorption curve taken at a linear ramp rate of 0.5 K s^{-1} up to 1200 K reveals desorptive release at $\sim 500 \text{ K}$ and an areal D retention of $1.3 \pm 0.3 \times 10^{21} \text{ m}^{-2}$. Following a single 1 s, 8 MW m^{-2} LIDS flash event, TPD was done on the sample to check how much D remained in the sample (dashed curve of Fig. 8). The data reveal that approximately 97% of D was desorbed by the laser pulse, with fairly modest power density. In the case of this 1 s laser pulse, no surface damage such as roughening, melting, cracking, or ablation is observed.

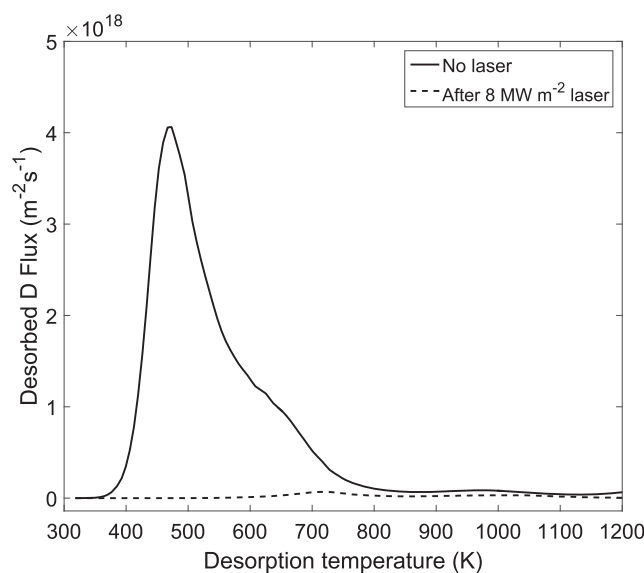


FIG. 8. TPD using a temperature ramp rate of 0.5 K s^{-1} for two W–D codeposits from the same deposition run (1.2 μm layer thickness with 330 K sample temperature), with no laser desorption (solid), and after 1 s laser desorption (dashed).

Confocal laser scanning microscope images of the W–D sample before and after laser irradiation show no change, indicating laser parameters which result in peak surface temperatures below the recrystallization temperature, but above a temperature of $\sim 900 \text{ K}$ at which nearly all D escapes, could be used for detritiation³⁴ with minimal impact on surface quality. However, if LIDS is performed repeatedly on the same area, thermomechanical properties may be affected due to creep or microcracks after a large number of thermal cycles.

The LIDS data of Fig. 7, generated by two successive laser irradiations show similar results to the conventional TPD data of Fig. 4, albeit on a more rapid time scale in the case of LIDS. The first 1 s shot in (a) at just under 10 MW m^{-2} leads to fast desorptive release at $\sim 500\text{--}700 \text{ K}$ in the calibrated deconvoluted Da signal, and the inferred areal D retention is $1.3 \pm 0.4 \times 10^{21} \text{ m}^{-2}$. The actual Da signal and the system response function are also shown for completeness. A subsequent shot (b) produces no further D release. It is pointed out that for the near full D removal from the target surfaces in each case (TPD and LIDS), the inferred measurements of D areal retention are in excellent agreement, thereby unequivocally demonstrating the viability of calibrated LIDS as a hydrogen isotope inventory measurement and a removal diagnostic tool. The LIDS signal-to-noise can be improved significantly in plasma sources with higher densities than those achievable in the rf plasma used here, allowing measurements of lower retention and higher temporal resolution through the use of shorter integration times on the spectrometer.

C. RF power and pressure scan

Use of the D_2 calibration leak for each plasma condition where LIDS is performed provides a direct method to quantify each LIDS D release independent of the plasma properties. The rf power and

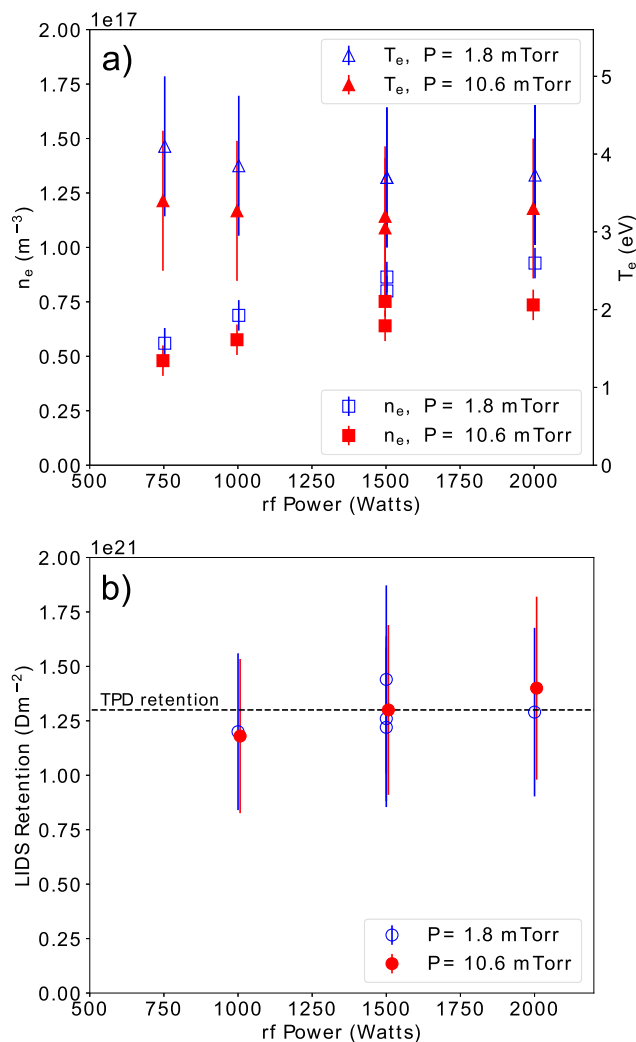


FIG. 9. Scan of rf power showing (a) electron density (squares) and temperature (triangles) for Ar fill pressures of 1.8 mTorr (blue) and 10.6 mTorr (red). (b) LIDS retention measurements from eight W–D codeposits all created from the same batch. Dashed line shows D retention of a sample from the same batch, measured using TPD.

argon fill pressure were varied in order to check this assumption, by investigating how changing plasma parameters would affect the LIDS measurement, if at all. Figure 9(a) shows the electron density and temperature, measured with a Langmuir probe located in the spectrometer viewing region at a distance of 28 cm above the sample, as a function of rf power. Three rf powers (1000, 1500, and 2000 W) and two argon fill pressures (1.8 and 10.6 mTorr) were investigated, resulting in a factor of 2 variation in electron density, n_e , and a factor of 1.3 variation in electron temperature, T_e . The LIDS retention measurements from W–D codeposits, shown in Fig. 9(b), were found to be relatively constant for all rf powers and Ar pressures, demonstrating, as expected, that the technique is robust to variations of these parameters, at least in the ranges explored.

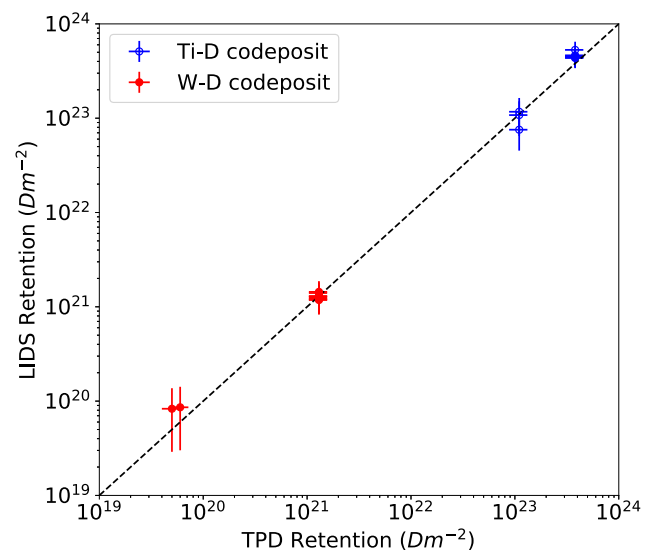


FIG. 10. Deuterium retention measured using LIDS compared with TPD, where the dashed line indicates one-to-one agreement.

A summary comparison of LIDS and TPD is shown in Fig. 10, showing agreement over nearly four orders of magnitude in measured areal D retention. The largest source of error in the 25 mm diameter Ti–D samples was uncertainty on the area of desorption, while at the low retention values of the two W–D samples, the error was due to low signal-to-noise ratio. That is, low signal limited the LIDS diagnostic in the present configuration to detection of a minimum of $\sim 10^{20}$ D m^{-2} ; however, higher density plasmas will be used in future work which will allow increased sensitivity. For the W–D codeposits near 1.3×10^{21} m^{-2} with full laser coverage, excellent agreement is seen between the LIDS and TPD measurements.

VI. SUMMARY

We have presented methods and techniques to analyze laser-desorbed particle flux measured using optical spectroscopy in a background plasma and applied those analysis methods to Ti–D and W–D codeposits in Ar plasma. The main contributions of this work are as follows: (1) Separate measurements of Da and Ha from separate D_2 and H_2 gas injections are obtained, which allows simultaneous determination of Da and Ha during LIDS using spectral fitting, (2) A calibrated leak of D_2 is used to convert the spectroscopic signal to particle flow rate. This requires the leak source to be located near the laser-irradiated surface. When this condition is met, the calibration is robust because precise knowledge of the spatially dependent plasma parameters along the spectroscopic line of sight is not needed, in contrast to the widely used S/XB method. In addition, the solid angle of light collection, optical transmission, and detector efficiency do not need to be known. More exotic methods of calibration could also be used in an actual fusion device, for example, a pellet filled with a known quantity of D_2 gas could be injected and then laser-ablated, providing a calibrated source of gas near the measurement location. (3) The system response function is measured experimentally using an impulsive burst of D_2 gas injection, and

numerical deconvolution of the LIDS signal with the system response function provides a correction for time-dependent system effects such as wall recycling and finite pumping speed. Note that recycling cannot be properly removed from the measured signal using other popular signal processing techniques such as background subtraction. The use of deconvolution is not limited to optical spectroscopic measurements, and can, for example, be used for mass spectrometry or any other time-resolved measurement of desorbed species.

ACKNOWLEDGMENTS

This work was supported by U.S. DOE Grant No. DE-SC0018281.

REFERENCES

- ¹R. P. Doerner, G. R. Tynan, and K. Schmid, *Nucl. Mater. Energy* **18**, 56 (2019).
- ²See http://science.energy.gov/~media/fes/pdf/workshop-reports/2016/PMI_fullreport_21Aug2015.pdf for Report on Scientific Challenges and Research Opportunities in Plasma Materials Interactions (PMI), FES Workshop on Plasma Materials Interactions.
- ³W. Möller and F. Besenbacher, *Nucl. Instrum. Methods* **168**, 111 (1980).
- ⁴M. Rubel *et al.*, *Nucl. Instrum. Methods Phys. Res., Sect. B* **371**, 4 (2016).
- ⁵V. Philipps *et al.*, *Nucl. Fusion* **53**, 093002 (2013).
- ⁶A. Huber, B. Schweer, V. Philipps, N. Gierse, M. Zlobinski, S. Brezinsek, W. Biel, V. Kotov, R. Leyte-Gonzales, Ph. Mertens, and U. Samm, *Fusion Eng. Des.* **86**, 1336 (2011).
- ⁷B. Schweer, G. Beyene, S. Brezinsek, N. Gierse, A. Huber, F. Irrek, V. Kotov, V. Philipps, U. Samm, and M. Zlobinski, *Phys. Scr.* **T138**, 014008 (2009).
- ⁸D. Nishijima, M. Patino, and R. P. Doerner, *Rev. Sci. Instrum.* **89**, 10J105 (2018).
- ⁹C. Grisolia, A. Semerok, J. M. Weulersse, F. Le Guern, S. Fomichev, F. Brygo, P. Fichet, P. Y. Thro, P. Coad, N. Bekris, M. Stamp, S. Rosanvallon, and G. Piazza, *J. Nucl. Mater.* **363-365**, 1138 (2007).
- ¹⁰C. Li, C.-L. Feng, H. Y. Oderji, G.-N. Luo, and H.-B. Ding, *Front. Phys.* **11**, 114214 (2016).
- ¹¹Q. Xiao, R. Hai, H. Ding, A. Huber, V. Philipps, N. Gierse, and G. Sergienko, *J. Nucl. Mater.* **463**, 911 (2015).
- ¹²L. Mercadier, J. Hermann, C. Grisolia, and A. Semerok, *J. Nucl. Mater.* **415**, S1187 (2011).
- ¹³A. Semerok and C. Grisolia, *Nucl. Instrum. Methods Phys. Res., Sect. A* **720**, 31 (2013).
- ¹⁴K. Piip, G. De Temmerman, H. J. van der Meiden, A. Lissovski, J. Karhunen, M. Aints, A. Hakola, P. Paris, M. Laan, J. Likonen, I. Jögi, J. Kozlova, and H. Mändar, *J. Nucl. Mater.* **463**, 919 (2015).
- ¹⁵P. Paris, K. Piip, A. Hakola, M. Laan, M. Aints, S. Koivuranta, J. Likonen, A. Lissovski, M. Mayer, R. Neu, V. Rohde, and K. Sugiyama, *Fusion Eng. Des.* **98-99**, 1349 (2015).
- ¹⁶N. Gierse, M. Z. Tokar, S. Brezinsek, T. F. Giesen, M. Hubeny, A. Huber, V. Philipps, A. Pospieszczyk, G. Sergienko, J. Wegner, Q. Xiao, U. Samm, and Ch. Linsmeier, *Phys. Scr.* **T167**, 014034 (2016).
- ¹⁷D. D. R. Summers, M. N. A. Beurskens, J. P. Coad, G. Counsell, W. Fundamenski, G. F. Matthews, and M. F. Stamp, *J. Nucl. Mater.* **290-293**, 496 (2001).
- ¹⁸B. Schweer, F. Irrek, M. Zlobinski, A. Huber, G. Sergienko, S. Brezinsek, V. Philipps, and U. Samm, *J. Nucl. Mater.* **390-391**, 576 (2009).
- ¹⁹M. Zlobinski, V. Philipps, B. Schweer, A. Huber, H. Stoschus, S. Brezinsek, and U. Samm, *Phys. Scr.* **T145**, 014027 (2011).
- ²⁰M. Zlobinski, V. Philipps, B. Schweer, A. Huber, S. Brezinsek, Ch. Schulz, S. Möller, and U. Samm, *Fusion Eng. Des.* **86**, 1332 (2011).
- ²¹F. Schwirzke, H. Brinkschulte, and M. Hashmi, *J. Appl. Phys.* **46**, 4891 (1975).
- ²²B. L. Doyle and F. L. Vook, *J. Nucl. Mater.* **85-86**, 1019 (1979).
- ²³C. H. Skinner, N. Bekris, J. P. Coad, C. A. Gentile, and M. Glugla, *J. Nucl. Mater.* **313-316**, 496 (2003).
- ²⁴K. Hirata, K. Furumoto, N. Yamamoto, and T. Tanabe, *J. Nucl. Mater.* **443**, 298 (2013).
- ²⁵B. Schweer, F. Irrek, G. Sergienko, V. Philipps, and U. Samm, *J. Nucl. Mater.* **363**, 1375 (2007).
- ²⁶M. Zlobinski, V. Philipps, B. Schweer, A. Huber, M. Reinhart, S. Möller, G. Sergienko, U. Samm, M. H. J. 't Hoen, A. Manhard, and K. Schmid, *J. Nucl. Mater.* **438**, S1155 (2013).
- ²⁷J. H. Yu, M. Simmonds, M. J. Baldwin, and R. P. Doerner, *Nucl. Mater. Energy* **12**, 749 (2017).
- ²⁸E. S. Marmar, *J. Nucl. Mater.* **76**, 59 (1978).
- ²⁹M. J. Weber, *Handbook of Optical Materials* (CRC Press, Boca Raton, 2003).
- ³⁰J. H. Yu, M. J. Baldwin, and R. P. Doerner, *Phys. Scr.* **T170**, 014009 (2017).
- ³¹J. H. Yu, G. De Temmerman, R. P. Doerner, and R. A. Pitts, *Nucl. Fusion* **55**, 093027 (2015).
- ³²Y. Hirooka, *J. Vac. Sci. Technol., A* **2**, 16 (1984).
- ³³M. J. Simmonds, J. H. Yu, Y. Q. Wang, M. J. Baldwin, R. P. Doerner, and G. R. Tynan, *J. Nucl. Mater.* **508**, 472 (2018).
- ³⁴G. De Temmerman *et al.*, *Nucl. Mater. Energy* **12**, 267 (2017).